Monte Carlo Simulations of Water under Supercritical Conditions. I. Thermodynamic and Structural Properties

A. G. Kalinichev *

Max-Planck-Institut für Chemie (Otto-Hahn-Institut), W-6500 Mainz, FRG

Z. Naturforsch. **46a**, 433–444 (1991); received January 7, 1991

The thermodynamic and structural properties of water along two supercritical isotherms at 673 and 773 K in the pressure range from 0.3 to 30 kbar have been studied by the NPT-ensemble Monte Carlo method using a TIP4P intermolecular pair potential. Simulated values of the configurational enthalpy, molar volume, isobaric heat capacity, isothermal compressibility, and thermal expansion coefficient are found to be in a rather good agreement with experimental data, although the critical point of the TIP4P water model is supposed to lie about 50 degrees lower than observed experimentally. The analysis of simulated atom-atom radial distribution functions as well as the dimerization energy distributions clearly shows that hydrogen bonding persists under the conditions studied, despite the fact that the water structure may be considered as "argon-like" in terms of oxygen-oxygen distribution functions (i.e. close to that of a simple liquid).

Key words: Monte Carlo computer simulation, Supercritical conditions, Thermodynamic properties, Water structure.

1. Introduction

In recent years the physical chemistry of aqueous solutions at high temperatures and pressures has become a subject of great scientific interest [1, 2]. Despite an increasing demand for data and models for aqueous solutions at high temperatures and pressures from various groups of scientists, ranging from geologists and environmentalists to chemical and nuclear power engineers, fundamental work has lagged far behind that devoted to solutions in ordinary liquid water [3]. The near-critical region of the phase diagram, where the properties of water as well as those of aqueous solutions undergo drastic changes in a very narrow range of temperatures and pressures [2, 3], seems to be of primary importance. Although computer simulation techniques (both Monte Carlo (MC) and Molecular Dynamics (MD)) have already proved to be one of the powerful tools to study usual aqueous solutions [4], these methods still have not been applied systematically over a wide enough range of thermodynamic conditions.

Even the solvent itself – pure water – has not yet been extensively studied by these methods at high temperatures and pressures from both thermodynamic and structural points of view, although several important exceptions should be mentioned in this context. In most studies either high pressures [5–9] or high temperatures [10–13] were applied to the system, where the term "high temperature" usually meant 373–473 K. Because of a relatively low compressibility and thermal expansivity of water under such conditions, only liquid-like densities have been studied.

O'Shea and Tremaine [14] have studied supercritical water at lower density. Kataoka [15] has made the most extensive simulation study of fluid water over a very wide range of the phase diagram. However, in both cases structural results were not reported. On the other hand, in MD simulations of Mountain [16] only radial distribution functions of expanded water at elevated temperatures were analysed.

In the present work an attempt has been made to simulate relatively low-density thermodynamics states of supercritical water and to study thermodynamic properties as well as the structure of water under these conditions. A variety of empirical [5, 7–13, 16] and non-empirical [6, 14, 15] intermolecular potential functions has already been tested in the above mentioned studies. The empirical TIP4P potential [17], which proved to be quite successful in describing properties of water over a range of temperatures [12] and pressures [8, 9] is used in the present work.

The technical details of the simulations are described in Section 2. In Sect. 3 the simulated thermodynamic properties are compared with available experimental data and the possible localization of the

* Alexander von Humboldt fellow; permanent address and reprint requests to Dr. A. Kalinichev, Institute of Experimental Mineralogy, USSR Academy of Sciences, 142432 Chernogolovka, Moscow District, USSR.

0932-0784 / 91 / 0500-0433 $ 01.30/0. – Please order a reprint rather than making your own copy.

critical point of the TIP4P water is discussed. In Sect. 4 bonding energy and dimerization energy distributions as well as the average potential energy of water-water interaction are analysed. The analysis of structural results is found in Sect. 5, followed by general conclusions in Section 6.

2. Methodology of the simulations

A cubic sample of N water molecules ($N=64$ or 216) with periodic boundary conditions was simulated at eight thermodynamic states along the 773 and 673 K supercritical isotherms in a pressure range from 0.3 to 30 kbar (1 kbar = 0.1 GPa). Rigid water molecules were interacting via the effective site-site pair potential TIP4P [17], which uses the experimental geometry of the monomer (OH bond length = 0.9572 Å and $\angle$ HOH = 104.52°) and has four interaction sites, three on the nuclei and one on a point M located on the bisector of the HOH angle at a distance of 0.15 Å from the oxygen towards the hydrogens. The hydrogens are assumed to have charges of $0.52\,e$, compensated by the charge $-1.04\,e$ on M. The total interaction energy for a pair of molecules a and b consists of the Coulomb interactions between the charged sites and a Lennard-Jones interaction between the oxygen atoms, and has the form

$$U_{ab} = \sum_{i}^{\text{on } a} \sum_{j}^{\text{on } b} \left(\frac{q_i\, q_j\, e^2}{r_{ij}} \right) + \frac{A}{r_{\text{OO}}^{12}} - \frac{C}{r_{\text{OO}}^{6}}. \qquad (1)$$

The Lennard-Jones parameters are $A = 2\,510\,400$ kJ Å^{12}/mol and $C = 2552$ kJ Å^6/mol (or $\sigma = 3.154$ Å and $\varepsilon/k = 78.1$ K in conventional LJ-units).

The minimum image principle [18] was applied to calculate the energy of the intermolecular interactions with a molecular cutoff criterium based on the coordinates of the oxygen atoms. No long-range corrections were made. It was shown [19] that this method leads to only small errors in the resulting thermodynamic properties and atom-atom radial distribution functions even with $N=64$. However, to check this, additional runs were performed at the lowest and highest densities studied with $N=216$ water molecules in the basic cell (and, hence, with an approximately 1.5 times larger cutoff distances). The run at the high density showed no significant deviations from the results obtained wih the smaller cell ($N=64$), while the low-density run has demonstrated a slight size dependence. For these two thermodynamic states only the results for the larger cell are reported here. The size effects of the simulations will be discussed in a separate paper [20].

All simulations were done using th conventional Monte Carlo algorithm for an isothermal-isobaric ensemble [18]. New configurations were generated by cyclically selecting a water molecule, translating it randomly along all three Cartesian axes, and rotating it randomly about one of the axes, again chosen at random. After random intervals, amounting in the average to n_V steps, the volume of the system was also changed by scaling all intermolecular distances.

The ranges of possible molecular displacement $\pm\delta l$, rotation $\pm\delta\phi$, and volume increments $\pm\delta V$ along with some other parameters of the present Monte Carlo runs are given in Table 1. These ranges were adjusted at the equilibration stage for each run to yield acceptance ratios from ca. 0.35 to ca. 0.5, and were monitored independently for translation-rotation and volume-changing moves.

After several runs at 298 K and 1 bar, which served to check the reproducibility of previous studies [12, 17], the simulations were carried out from the highest density to the lowest one to ease the equilibration at each new thermodynamic state. In every case not less than 0.5×10^6 equilibration configurations were discarded before the averaging over the Markov chain. The lengths of configuration chains for each run are also given in Table 1.

To check the consistency with our previous simulations under supercritical conditions [21] several runs were made with the TIPS2 intermolecular potential which has the same geometry and functional form (1), but slightly different point charges and Lennard-Jones

Table 1. Main parameters of the Monte Carlo runs.

Run	T/K	P/kbar	N	n_V	Configs. $\times 10^{-6}$	δl/Å	$\delta\phi$/°	δV/Å^3
1 [a]	298	0.001	64	128	3.20	0.15	15	60
2	298	0.001	64	128	3.20	0.15	15	60
3 [a]	773	30	64	128	1.10	0.18	22	65
4	773	30	64	128	1.10	0.18	22	65
5	773	30	216	432	1.10	0.21	27	180
6	773	10	64	128	0.37	0.20	30	125
7 [a]	773	1	64	128	1.10	0.55	55	480
8	773	1	64	128	1.60	0.48	60	375
9	773	0.5	64	128	1.10	0.87	65	1570
10	673	10	64	128	1.10	0.23	35	140
11	673	1	64	128	1.10	0.46	45	310
12	673	0.5	64	32	1.60	0.40	60	750
13	673	0.3	216	216	1.60	0.61	110	3400

[a] With the TIPS2 potential.

Table 2. Thermodynamic results of Monte Carlo simulations.

Run	T K	P kbar	$\langle V_m \rangle$ (cm^3/mol)		$\langle H \rangle$ (kJ/mol)		C_P (J/(mol · K))		$\varkappa$ (1/Mbar)		α (10^{-3}/K)	
			MC	HGK[a]	MC	HGK[a]	MC	HGK[a]	MC	HGK[a]	MC	HGK[a]
5	773	30.000 (25.692)[b]	14.03 ± 0.02	13.52	12.35 ± 0.10	15.17 (9.87)	56.0 ± 2.2	61.4	6.7 ± 0.5	8.0	0.25 ± 0.03	0.12
6	773	10.000 (8.454)	18.20 ± 0.05	17.51	−8.91 ± 0.18	−9.55 (−11.37)	63.9 ± 5.2	63.6	32.7 ± 3.5	23.1	0.66 ± 0.08	0.41
8	773	1.000 (0.721)	43.13 ± 0.67	34.11	−11.53 ± 0.22	−14.70 (−12.29)	92.5 ± 4.6	100.1	780 ± 70	543.0	3.4 ± 0.3	3.28
9	773	0.500 (0.450)	83.34 ± 1.70	70.11	−6.07 ± 0.22	−7.35 (−5.75)	86.2 ± 5.3	130.4	2520 ± 340	3263.0	4.2 ± 0.4	7.06
10	673	10.000 (9.131)	17.12 ± 0.04	16.82	−13.14 ± 0.13	−12.98 (−14.05)	64.0 ± 2.3	63.9	19.7 ± 1.3	19.8	0.50 ± 0.04	0.39
11	673	1.000 (0.497)	31.23 ± 0.53	26.01	−18.39 ± 0.29	−21.22 (−19.70)	95.1 ± 7.3	88.5	420 ± 50	211	3.1 ± 0.4	2.14
12	673	0.500 (0.306)	47.21 ± 0.99	31.17	−14.60 ± 0.25	−19.72 (−15.39)	122.4 ± 7.7	122.3	1680 ± 160	713	6.2 ± 0.6	4.89
13	673	0.300 (0.264)	89.70 ± 1.50	50.31	−9.04 ± 0.18	−14.74 (−8.86)	116.3 ± 10.8	451.8	4500 ± 600	11712	7.25 ± 1.0	36.75

[a] Values calculated from the HGK equation of state for water [23] are given for comparison as "experimental".
[b] In parentheses the HGK-values for the pressure and the configurational enthalpy at the simulated densities are given.

parameters [22]. As in the case of simulations at normal conditions [17], runs 4 and 8 with the TIP4P potential have shown somewhat better thermodynamic results than simulations with the TIPS2 model (runs 3 and 7, respectively), while all other results, such as radial distribution functions, bonding and pair energy distributions, turned out to be virtually identical within the limits of statistical uncertainties. Therefore, only the results for the TIP4P model are discussed further.

3. Thermodynamic Properties

The calculated values of configurational enthalpy, molar volume, isobaric heat capacity, and coefficients of isothermal compressibility and thermal expansion for all thermodynamic states studied are reported in Table 2. Thermodynamic properties calculated via the HGK equation of state for water [23], approved by the International Association for the Properties of Steam (IAPS) as an international standard up to 1273 K and 10 kbar are also given in Table 2 for comparison. This equation reproduces virtually all available thermodynamic measurements within the limits of their experimental accuracy and is used in the present study as a reliable source of self-consistent "experimental" data.

The molar configurational enthalpy was estimated from the equation of state by

$$H_{\text{conf.}} = H(T, P) - H_{\text{i.g.}}(T) + RT \qquad (2)$$

with the ideal gas reference state at the given temperature. The constant $3R$ was added to the simulated values of C_P for the classical kinetic energy contribution from translation and rotation of molecules. No other corrections were added to any property reported.

The statistical uncertainties ($\pm 1\,\sigma$) of the thermodynamic properties reported here were calculated from separate averages over batches of 64 000 configurations. These batches are supposed to be large enough to get reasonable estimates of uncertainties for all the properties, except, possibly, thermal expansion coefficients. A more detailed discussion of the statistical error estimations along with the convergence analysis will be given elsewhere [20].

Molar volume. The comparison of simulated and experimental molar volumes is presented in Table 2, and in Fig. 1 a graphical representation of the two density isotherms is shown. The good agreement of calculated ($\langle V_m \rangle$) and experimental volumes for runs 5, 6 and 10 cannot be considered as surprising, because the TIP4P potential has already been carefully tested at liquid-like and higher densities up to 373 K [12], and up to 10 kbar at 298 K [9]. In the very recent MD simulations [24] the TIP4P potential was successfully used even at a density almost twice as high as the normal one and at a temperature of about 2000 K.

At lower densities (pressures), the simulated volumes become systematically higher than the experimental ones. The reason for the agreement with exper-

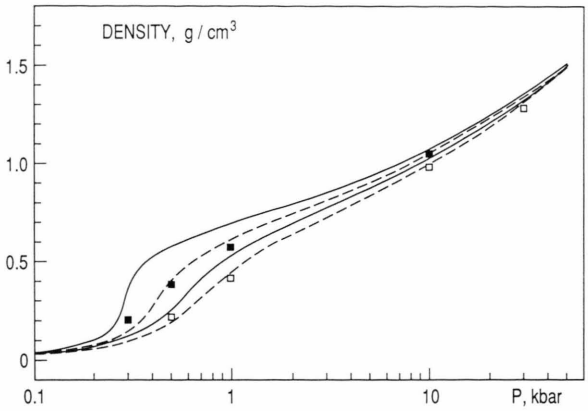

Fig. 1. Simulated (squares) and HGK [23] (curves) isotherms of water density. Filled symbols, 673 K; open symbols, 773 K. Full lines, 673 and 773 K; dashed lines, 723 and 823 K.

iment in the first case, and for the discrepancy in the second, most probably lies in the "effective" nature of the TIP4P potential, which was specially developed to reproduce correctly thermodynamic and structural properties of liquid water under normal conditions and implicitly includes many-body effects of intermolecular interactions [17]. The relative influence of these effects should obviously be density-dependent, which is not readily taken into account by the present potential model and may lead to increasing disagreement with experimental values as density decreases. The same conclusion can be drawn from the results of De Pablo and Prausnitz [13] who made Gibbs-ensemble Monte Carlo simulations of TIP4P water along the vapor-liquid coexistence curve. They noted that vapor densities are predicted less accurately then liquid ones, and that the agreement with experiment deteriorates rapidly as the temperature rises to ca. 500 K.

At 673 K and 0.3 kbar (run 13) the simulated volume is almost twice as large as the experimental one. In this thermodynamic state the water density changes drastically in a very narrow interval of pressure around 0.3 kbar (Fig. 1) because of the extremely high supercritical compressibility (see below). Therefore, the observed discrepancy between simulated and experimental densities may not only be due to the reasons mentioned above. It may be simply an indication of the lower critical temperature of TIP4P water, compared with the experimental value of 647 K. The tendency toward such behaviour is clearly seen from the simulated density isotherms in Fig. 1, which do not show the characteristic inflection with the rapid change of density around it. The shape of the simulated isotherms corresponds more closely to higher temperature isotherms of water (such curves for 723 and 823 K are shown on Fig. 1 as dashed lines), suggesting that the critical point of TIP4P water may lie about 50–70 degrees lower than the experimental one. The same assumption can be made from the recently published data on the coexistence curve of TIP4P water [13]. Estimates for the empirical SPC potential [25] also give lower critical density and temperature [26].

The failure to reproduce critical parameters correctly seems to be a general feature of any empirical potential, which is parameterized to describe the properties of water at liquid-like densities. The reason for this lies in the above mentioned "effective" nature of such potentials, which only implicitly include many-body effects. Indirect confirmation of this statement can be found in the work of Kataoka [15], who estimated the critical temperature to be about 50 degrees lower (as well as somewhat lower critical density) for the nonempirical Carravetta-Clementi pair potential of water [27], which does not include many-body effects neither explicitly, nor implicitly.

It is interesting to note that in their simulations of the ice-water interface Karim and Haymet [28] also found the freezing point of TIP4P water to be about 35 degrees lower than the experimental value. On the other hand, it is known [29] that exactly three- and higher-body interactions act to keep ice solid above the melting point for "hypothetical ice" in which only pair interactions were operative.

However, the phase diagram for any of the widely used potential models of water is still unknown over a sufficient range of temperatures and pressures*. The isothermal-isobaric Monte Carlo simulation used in the present work seems to be ineffective for this task because of the very large fluctuations of thermodynamic properties during a MC run close to the critical point [20], and the Gibbs-ensemble simulation method [30] used by De Pablo et al. [13, 26] may be preferable. The elegant technique of block density distributions, proposed recently by Rovere et al. [31] for the calculation of the phase diagram of the two-dimensional Lennard-Jones fluid and for the localization of its critical point in MC simulations, would demand enormous computational efforts in the case of

* The very recent study [26] is the first step in this direction.

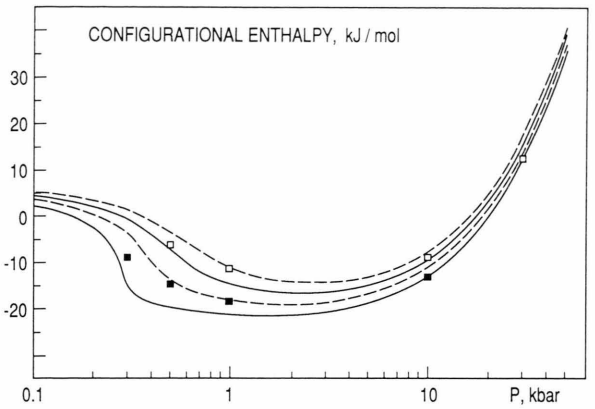

Fig. 2. Simulated (squares) and HGK [23] (curves) isotherms of configurational enthalpy. Filled symbols, 673 K; open symbols, 773 K. Full lines, 673 and 773 K; dashed lines, 723 and 823 K.

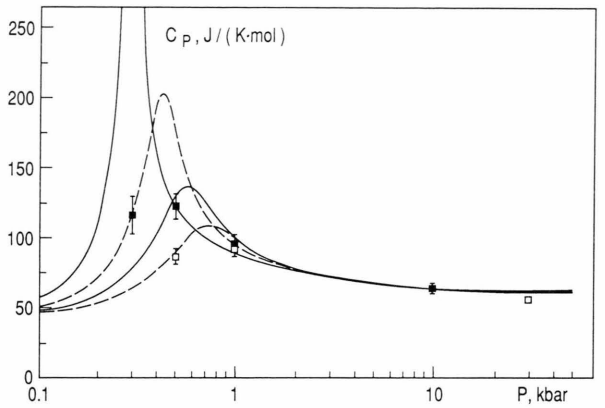

Fig. 3. Simulated (squares) and HGK [23] (curves) isotherms of heat capacity. Filled symbols, 673 K; open symbols, 773 K. Full lines, 673 and 773 K; dashed lines, 723 and 823 K.

three-dimensional water simulations with any realistic intermolecular potential.

Enthalpy. As in the case of the molar volume, the simulated values of configurational enthalpy ($\langle H\rangle = \langle U + PV\rangle$) show very good agreement with experiment at near-liquid water densities (see Table 2 and Figure 2). Here again, agreement rapidly deteriorates as pressure (and hence density) decreases. However, if the calculated densities are taken instead of pressures as the basis for comparison with experiment, the agreement still remains good at lower densities. That is, in constant-volume MC or MD simulations the TIP4P potential can reproduce correct values of enthalpy (or internal energy) over the whole density-temperature range studied at the price of error in pressure. Experimental values of pressure, corresponding to these simulated densities, are also given in Table 2 for comparison.

The agreement with the HGK equation of state also deteriorates somewhat at the highest pressure of 30 kbar (run 5). This point lies, however, beyond the approved limits of reliability for the HGK equation, and recent studies [32] show that the equation becomes increasingly inconsistent with shock wave measurements at such high pressures. It can therefore be concluded that the TIP4P water model reproduces, with reasonable accuracy, both the temperature and the density dependencies of enthalpy over a very wide range of thermodynamic parameters.

Isobaric heat capacity. The values of C_P were calculated via the standard formula for the fluctuation of enthalpy:

$$C_P = (\langle H^2\rangle - \langle H\rangle^2)/N k_B T^2. \quad (3)$$

Statistical uncertainties are much larger here, as compared with molar volume and enthalpy calculations which were computed directly during the run. However, even in this case, the agreement with experiment at liquid-like densities is again excellent, and becomes significantly worse only at the supercritical maxima of heat capacity for both isotherms (Figure 3).

As in the case of densities and enthalpies, the position of experimental 723 and 823 K isotherms (dashed lines on Fig. 3) suggests that the thermodynamic properties of TIP4P water are shifted down in temperature. The absence of the sharp maximum of C_P on the simulated 673 K isotherm clearly indicates that the critical point for this water model lies at least 50 degrees lower than the real one.

Confirmation of this assumption can be observed in the behaviour of the *isothermal compressibility* (Fig. 4), although relative statistical errors here are even larger than for C_P. This is quite understandable, considering the fluctuation formula for compressibility:

$$\varkappa = -\frac{1}{V}\left(\frac{\partial V}{\partial P}\right)_T = (\langle V^2\rangle - \langle V\rangle^2)/N k_B T \langle V\rangle, \quad (4)$$

and keeping in mind that the volume is changed less frequently than is the enthalpy during a Monte Carlo run. Agreement with experiment is, however, still quite good, considering that the compressibility changes by

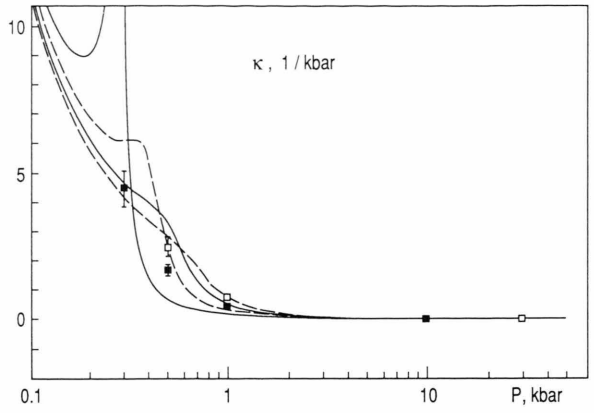

Fig. 4. Simulated (squares) and HGK [23] (curves) isotherms of compressibility. Filled symbols, 673 K; open symbols, 773 K. Full lines, 673 and 773 K; dashed lines, 723 and 823 K. The supercritical maximum of the compressibility at 673 K and 0.3 kbar is out of scale of the picture.

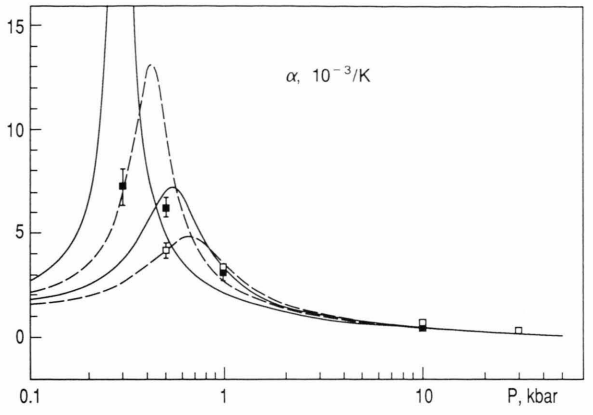

Fig. 5. Simulated (squares) and HGK [23] (curves) isotherms of thermal expansivity. Filled symbols, 673 K; open symbols, 773 K. Full lines, 673 and 773 K; dashed lines, 723 and 823 K.

several orders of magnitude between different runs (see Table 2 and Figure 4). Once again, the simulated isotherms at 673 and 773 K are much closer to the experimental 723 and 823 K isotherms, respectively (dashed lines on Figure 4).

Realistic statistical errors for the *thermal expansion coefficient* are difficult to estimate, because it is calculated as the cross-fluctuation of the enthalpy and the volume:

$$\alpha = \frac{1}{V}\left(\frac{\partial V}{\partial P}\right)_P = (\langle HV\rangle - \langle H\rangle\langle V\rangle)/N k_B T^2 \langle V\rangle, \quad (5)$$

and the convergence of this property in NPT-ensemble MC simulations is known to be very slow [33]. We shall discuss this problem in detail elsewhere [20], though it is worth noting here that the agreement of simulated values with experiment (Table 2 and Fig. 5) remains quite reasonable. This confirmes once again the assumption that the critical point for TIP4P water may lie at lower temperature (Figure 5).

In accordance with our earlier simulations for TIPS2 water [21], the simulated thermal expansion coefficient at 30 kbar was found to be approximately twice as large as calculated by the HGK equation of state [23]. It was suggested [21], that HGK equation may be incorrect in the region above ≈ 20 kbar, because none of the existent shock wave data at high pressures and temperatures were taken into account during its parametrization. This assumption has been confirmed now in the work of Saul and Wagner [32], who have shown that the HGK equation can even lead to negative values of the thermal expansion coefficient at higher pressures. Therefore the values of α given in Table 2 as "experimental" may be considered as underestimated at 30 kbar.

As a conclusion from the above analysis one can state that the TIP4P intermolecular potential reproduces thermodynamic properties of water with rather good accuracy over a much wider range of temperatures and pressures than was previously known [12, 9]. At the same time, at densities significantly lower than that of normal liquid water, all thermodynamic properties of TIP4P water seem to be shifted down in temperature by about 50 degrees (dashed lines on Figs. 1–5). Extrapolating the present simulation data one can estimate that the critical temperature and pressure for this water model are about 50–70 degrees and 50–70 bars lower than experimental T_c and P_c, respectively.

4. Potential Energy Distributions

Computer simulations provide a unique possibility to obtain detailed thermodynamic information on properties which are not readily studied by experiment. One such property is the bonding energy which represents the energetic environment experienced by a single water molecule.

Bonding energy distributions for every thermodynamic state presently studied are shown in Figure 6a, b. The effect of pressure on the distribution along

each isotherm is clearly seen from these curves. As in the case of normal temperature [9], the maximum of the distribution shifts to lower energies and its width increases with increasing pressure. It is interesting to note that especially under the high-temperature conditions a certain number of molecules even has a positive bonding energy. As the fraction of such molecules obviously cannot increase significantly with decreasing pressure, an asymmetry of the distribution at the lowest densities on each isotherm results.

It follows from the distribution asymmetry that the new simple and computationally efficient method of estimating the free energy in molecular simulations [34] cannot be applied to low-density aqueous systems, because this method essentially uses the tendency of all energy-related quantities toward a normal distribution. However, the test particle method (see [18] for a review) may be used efficiently at low densities.

The bonding energy distribution of water monomers in normal liquid water is shown as the dashed line in the Figure 6a. At 773 K and 10 kbar the density of supercritical water is virtually the same (≈ 1 g/cm^3) as that of liquid water at 298 K and 1 bar. Therefore, the difference between two distributions (curves 1 and 3 in Fig. 6a) can be considered as purely an effect of temperature. At high temperature the distribution shifts by about 40 kJ/mol to higher (less negative energies and becomes significantly wider. This effect has already been noted at temperatures up to 373 K along the vapor-liquid coexistence curve [12], where it could, however, be considered as a common effect of the increased temperature and decreased density. The comparison of both distributions clearly shows that a water molecule experiences completely different energetic environments in these two thermodynamic states despite the fact that the densities (and hence average intermolecular distances) are virtually the same in both cases.

As the density differences between runs 6, 8, 9 at 773 K and runs 10, 12, 13 at 673 K, respectively, amount to only about 10% (see Table 2), one can conclude from comparisons of curves 3(a) and 1(b), 4(a) and 3(b), 5(a) and 4(b) in Fig. 6 that the bonding energy distributions show almost no temperature dependence in the supercritical temperature range studied.

Pair energy distributions are another type of microthermodynamic information easily obtainable from computer simulations. Such functions, which represent the distribution of dimer energies, are shown in Fig. 7 for all thermodynamic states studied. Under supercritical conditions considered here the temperature is too high to obtain the well known bimodal distribution that one would expect for liquid water [12]. (The dotted line in Fig. 7a represents the distribution of pair energies in normal liquid water for comparison.) Though the maximum at low energies, which reflects the hydrogen-bonded neighbours, has already completely disappeared, a distinct shoulder is clearly seen in the same range of energies and indicates that hydrogen bonding persists to some extent under the conditions studied. As one would expext, this shoulder is more pronounced at the lower temperature (Fig-

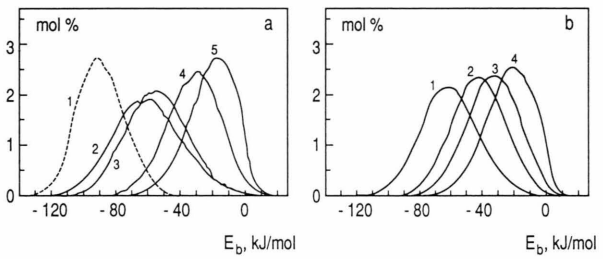

Fig. 6. Normalized distributions of total intermolecular bonding energies for monomers in supercritical water. a: 773 K; 2, 30 kbar; 3, 10 kbar; 4, 1 kbar; 5, 0.5 kbar. The dashed line represents the distribution for liquid water at normal conditions. b: 673 K; 1, 10 kbar; 2,1 kbar; 3, 0.5 kbar; 4, 0.3 kbar. Units for the ordinate are mole percent per kJ/mol.

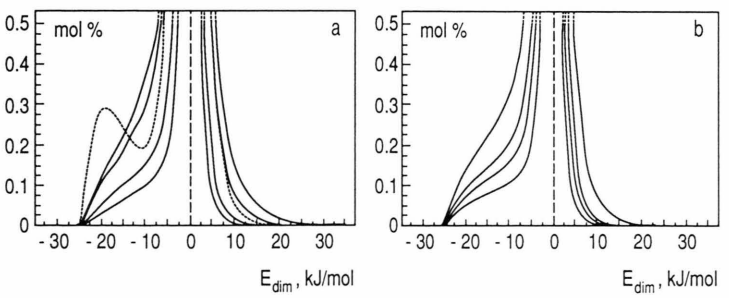

Fig. 7. Normalized distribution of pair interaction energies (dimerization energies) in supercritical water. a: 773 K; full lines (from the top to the bottom), 30, 10, 1, and 0.5 kbar. The dotted line represents the distribution for liquid water under normal conditions. b: 673 K; full lines (from the top to the bottom), 10, 1, 0.5, and 0.3 kbar. Units for the ordinate are mole percent per kJ/mol.

ure 7 b). As the pressure (density) decreases along each isotherm, the distributions become narrower with higher maxima (beyond the scale in Fig. 7), because more pairs of molecules have near-zero interaction energy at long distances.

The comparison of distributions at 773 K and 10 kbar and at 298 K and 1 bar (the second curve form the top and the dotted curve in Fig. 7 a, respectively) gives once again the opportunity to see the pure effect of a significant temperature increase on the shape of the distribution along an isochore, as the densities at both thermodynamic states are virtually equal. The width and the height of the main maximum remains unchanged. However, in the attractive branch of the distribution (negative energies) a significant amount of interacting molecular pairs are redistributed from the "hydrogen-bonding" range of energies ($\approx -25 - -15$ kJ/mol) to the "non-bonding" range ($\approx -15 - -6$ kJ/mol). In the repulsive (positive) branch the probability for a molecular pair to have a rather high interaction energy between 10 and 20 kJ/mol noticeably increases, confirming that repulsive interactions are a more important contribution to the thermodynamics of water at high temperatures.

It is concluded that profound changes take place in the neighbourhood about a molecule as the temperature significantly increases, despite the virtually unchanged density and, consequently, unchanged average intermolecular distances. However, the distribution of intermolecular distances is also changed dramatically under the conditions studies, as will be shown in the next section, where the structure of supercritical water is discussed.

Curves representing the distance dependence of the *average potential energy* of pair interaction $\langle U(r) \rangle$ are also a source of helpful information characterizing the energetic environment of a single water molecule [7]. These functions at 773 K and several pressures are shown in Figure 8 a. One can also separate coulombic and non-coulombic contributions to them. However, the only non-coulombic contribution to the water-water interaction in TIP4P intermolecular potential is the oxygen-oxygen Lennard-Jones term (see (1)) and, hence, its contribution to $\langle U(r) \rangle$ is both temperature- and density-independent (shown in Fig. 8 b as the dotted line). Therefore, in contrast to simulations with the BJH intermolecular potential [35], where changes with pressure in both coulombic and non-coulombic components of the average potential energy take place [7], in the case of the TIP4P potential only the change

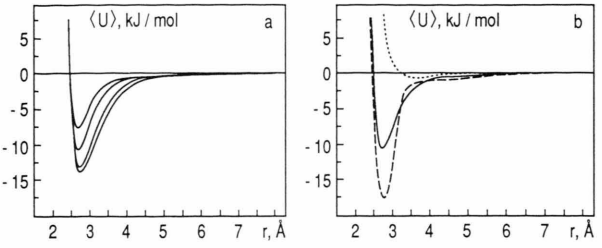

Fig. 8. Distance dependence of the averaged potential energy between two water molecules for supercritical water. a: 773 K and 30, 10, 1, and 0.5 kbar (from the top to the bottom). b: full line, 773 K and 10 kbar; dashed line, 298 K and 0.001 kbar. The water density is virtually the same in both thermodynamic states. Dotted line, non-coulombic contribution to $\langle (U(r) \rangle$.

of the coulombic part determines the behaviour of the whole function. The general trend for both isotherms is that as the pressure (density) decreases, the coulombic attraction becomes stronger (more negative) giving rise to the deepening of the average potential energy. The same trend for the flexible BJH potential has been noted already under high-pressure, low temperature conditions [7]. One can assume, therefore, that in order to reproduce thermodynamic properties of supercritical water with some kind of effective spherically symmetric potential, density dependent parameters of the potential might be necessary.

Along with bonding energy distributions (Fig. 6) these functions give one more possibility to analyse an average energetic environment experienced by a single water molecule under various thermodynamic conditions. The full and the dashed lines in Fig 8 b represent, respectively, the distance dependence of the average potential energy for supercritical water at 773 K and 10 kbar, and that for liquid TIP4P water under normal conditions. It can be concluded from the comparison of the curves that, as the temperature increases, the average energetic environment of a water molecule changes drastically (together with the distribution of intermolecular distances; see below), despite the fact that the average intermolecular distances remain unchanged because of the constant density. The shallow minimum around 4.5 Å in the coulombic part of $\langle (U(r) \rangle$, which is responsible for tetrahedric ordering of molecules in liquid water, and which remains unchanged even for high-density water at relatively low temperature of 350 K [7], completely disappears under supercritical conditions. The position of the potential well remains virtually unchanged while its depth decreases significantly, indicating that, on the

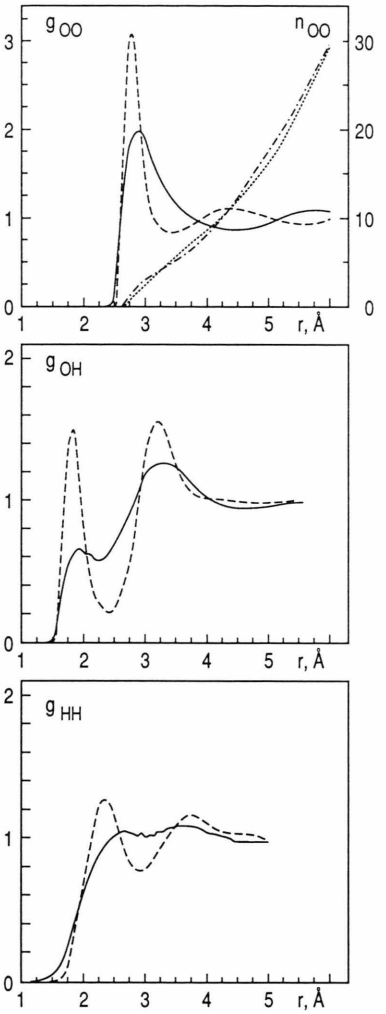

Fig. 9. Temperature dependence of atom-atom radial distribution functions. Full lines, 773 K and 10 kbar; dashed lines, 298 K and 0.001 kbar. The water density is virtually the same in both thermodynamic states. Dotted and dash-dotted lines represent running coordination numbers for the high-temperature and low-temperature states, respectively.

average, water molecules are bonded to each other almost twice as weakly under supercritical conditions than in normal liquid water, despite only minor differences in density between both thermodynamic states.

5. Structural Results

Oxygen-oxygen, oxygen-hydrogen, and hydrogen-hydrogen radial distribution functions (RDFs) for 773 K and 10 kbar, where supercritical water has the same density as liquid water under normal conditions, are shown in Fig. 9 (full lines). Dashed lines represent the results of simulations at 298 K and 1 bar. Running coordination numbers, calculated as

$$n(r) = 4\pi\varrho \int_0^r r^2 g_{OO}(r)\,dr, \tag{6}$$

are also shown in Fig. 9 as dotted and dash-dotted lines for high-temperature and low-temperature conditions, respectively.

The structure of water changes dramatically as the temperature significantly increases, even at liquid-like density. The characteristic second maximum of oxygen-oxygen RDF at $\approx$4.5 Å, reflecting the tetrahedral ordering of water molecules due to hydrogen bonding, is completely absent under supercritical conditions. Moreover, a pronounced minimum of the distribution appears in its place. The comparison of the $g_{OO}(r)$ and $n(r)$ functions at low and high temperatures shows that a significant redistribution of first and second neighbours from "hydrogen-bonding" regions of $\approx$2.7–2.9 Å and $\approx$3.8–5.0 Å to the intermediate "non-bonding" region of $\approx$3.1–3.8 Å takes place. As was recently shown [36], exactly the pairs of water molecules at intermediate distances are primarily responsible for repulsive interactions. Therefore, additional molecular density at these distances gives rise not only to the increase of weakly bonded molecular pairs, but to the increase of repulsive interactions as well (see Fig. 7 and the discussion of pair interaction energy distributions in Section 4).

The sharp first peak of $g_{OH}(r)$ in normal liquid water becomes significantly lower and much more diffused under supercritical conditions, though its presence indicates that hydrogen bonding persists at 773 K. Hydrogen-hydrogen correlations almost completely disappeared at this temperature (Figure 9).

In Fig. 10 the oxygen-oxygen, oxygen-hydrogen, and hydrogen-hydrogen RDFs for all the studied states are shown. Available experimental data on X-ray diffraction of water under supercritical conditions at 1 kbar pressure [37] are also shown as dashed lines in Fig. 10 a, d for comparison. Though the agreement is sufficiently satisfactory to the heights of the first maximum and the general shape of the curves, the disagreement in the positions of the main maximum and the different steepness of repulsive branches of the curves are rather disappointing. To some extent, this may be the result of the lower simulated densities at the experimental pressure of 1 kbar. However, the

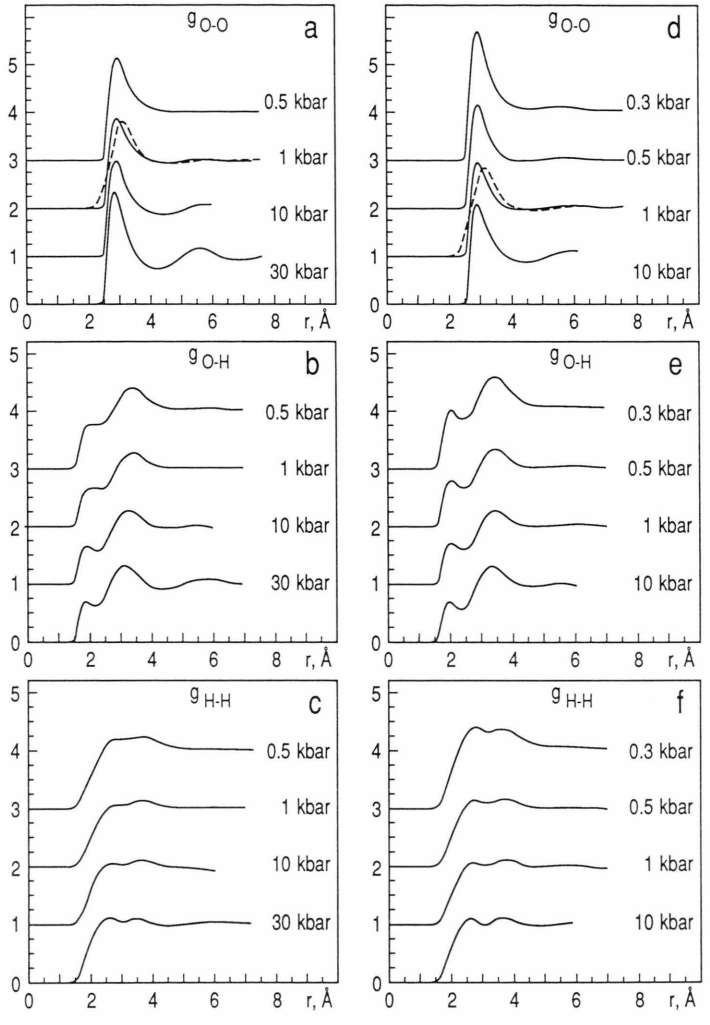

Fig. 10. Simulated atom-atom radial distribution functions (full lines) for supercritical water at 773 K (a, b, c) and 673 K (d, e, f). Dashed lines represent X-ray diffraction measurements [37] under the same conditions.

comparison of simulated RDFs at normal conditions with experimental data [37] shows a similar discrepancy in the steepness at small distances. Recent determination of the water structure from neutron diffraction experiments [38] also gives a less steep repulsion branch of the RDF. Unfortunately, the latter data exist only for normal liquid water at 298 K, and the reason of the present discrepancy, therefore, requires a more thorough analysis, which will be pursued in a subsequent study.

The general distance-, temperature-, and density-dependence of $g_{OO}(r)$ (Fig. 10a, d) in the whole pressure-temperature range studied, closely resembles that of a simple liquid with second maxima at distances approximately twice as large as the first. Little can be said about the behavior of $g_{HH}(r)$ (Fig. 10c, f), except for a simple general notion that these functions show almost no H – H correlations under supercritical conditions. The shape of $g_{OH}(r)$ (Fig. 10b, e) remains virtually the same along both isotherms over a very wide range of pressures from 0.3 to 30 kbar. The small first peak at ≈ 1.8 Å indicates that hydrogen bonding still persists at all temperatures and densities studied.

Because of the diffuseness of the first peak of $g_{OH}(r)$, a simple geometrical way to calculate the number of hydrogen bonds by integrating $g_{OH}(r)$ up to 2.4 Å (the position of the first minimum of $g_{OH}(r)$ in normal liquid water), proposed by Mountain [16],

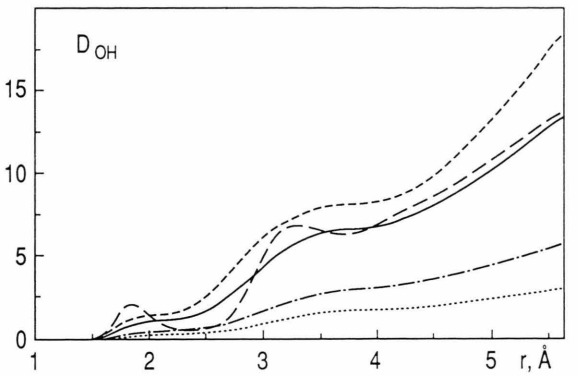

Fig. 11. Distribution functions of the atomic density $D_{OH}(r)$ at 773 K. Dashed line, 30 kbar; full line, 10 kbar; dash-dotted line, 1 kbar; dotted line, 0.5 kbar. The long-dashed line represents the same function for liquid water under normal conditions.

seems hardly adequate under the conditions studied. A more detailed geometric interpretation of the coordination number in water [37], based on the approximation of the radial distribution function of particle density, $D(r)=4\pi\varrho r^2 g(r)$, by several Gaussian functions, also could be useful for hydrogen bonding analysis. Such functions, calculated from simulations a 773 K, as well as under normal conditions, are shown in Figure 11. It is clearly seen that, although there exist two distinct coordination spheres in normal liquid water and both methods mentioned above are easily applicable, a purely geometrical definition of hydrogen bonding is insufficient at supercritical temperatures where two coordination spheres overlap significantly. In this case a more complex analysis based both on geometrical and energetic criteria has to be done.

6. Conclusions

The results presented here show that thermodynamic and structural properties of supercritical water can be simulated with reasonable precision over a very wide pressure range from 0.3 to 30 kbar using the TIP4P intermolecular pair potential. At liquid-like densities the simulated values of configurational enthalpy, molar volume, isobaric heat capacity, isothermal compressibility, and thermal expansion coefficient are found to be in good agreement with experimental data, and the agreement remains reasonable in high- and low-density regions. However, the shape of both simulated isotherms (673 and 773 K) for all calculated properties leads one to the suggestion that the thermodynamic properties of the TIP4P water model are shifted down in temperature by about 50 degrees, and that the critical point for this water model is, correspondingly, 50–70 degrees and 50–70 bars lower than the experimental values.

The reason of this discrepancy at low densities lies, most probably, in the "effective" nature of the empirical intermolecular potential used, which was originally parameterized to reproduce correctly a set of liquid water properties under normal conditions [17], and which takes into account many-body effects of intermolecular interactions only implicitly. This conclusion seems to be consistent with the results of other simulations [13, 15, 26, 28], where different empirical or non-empirical two-body potentials were used in a wide enough range of temperatures and densities. However, the direct successive inclusion of three- and higher-body terms from ab initio calculations [39], though very impressive, can hardly be considered cost-effective in terms of computer time for most large-scale simulations, and such possibilities like reparametrization of empirical potentials for various ranges of temperature and density seem to be preferable.

Under supercritical conditions, the water structure (in terms of the oxygen-oxygen radial distribution function, which is dominating the structure of water) may be considered as "argon-like", i.e. close to that of a simple liquid, over the whole density range studied. However, pair energy distributions and the average potential energy of intermolecular interactions as well as O–H radial distribution functions clearly show that Coulombic interactions at short distances still play an important role and the hydrogen bonding persists even at such high temperatures as presently studied. Therefore any analytical approach to the thermodynamics and structure of supercritical water cannot be based on a simple spherically symmetric intermolecular potential as was suggested previously [21]. Recent careful analysis of electrostatic and packing contributions to the structure of liquid water [40] has shown that three terms covering separately the short range repulsion, the region of the potential minimum, and the long range electrostatic interactions must be taken into consideration and treated by a different theoretical approach. This seems still to be valid for the supercritical conditions studied in the present work.

Acknowledgement

The study has been carried out during a research stay at the Max-Planck-Institut für Chemie (Otto-Hahn-Institut) supported by the Alexander von Humboldt-Stiftung. The support and valuable discussions with Dr. K. Heinzinger are gratefully acknowledged.

[1] D. T. Rickard and F. E. Wickman, eds., Chemistry and Geochemistry of Solutions at High Temperatures and Pressures, Pergamon Press, Oxford 1981.
[2] E. U. Franck, Pure and Appl. Chem. **59,** 25 (1987).
[3] J. M. H. Levelt Sengers, Int. J. Thermophys. **11,** 399 (1990).
[4] K. Heinzinger, Molecular dynamics simulations of aqueous systems, in: Computer Modelling of Fluids Polymers and Solids (C. R. A. Catlow et al., eds.). Kluwer Academic Publishers 1990, pp. 357–394.
[5] F. H. Stillinger and A. Rahman, J. Chem. Phys. **61,** 4973 (1974).
[6] R. W. Impey, M. L. Klein, and I. R. McDonald, J. Chem. Phys. **74,** 647 (1981).
[7] G. Jancso, P. Bopp, and K. Heinzinger, Chem. Phys. **85,** 377 (1984).
[8] M. Rami Reddy and M. Berkowitz, J. Chem. Phys. **87,** 6682 (1987).
[9] J. D. Madura and B. M. Pettitt, D. F. Calef, Mol. Phys. **64,** 325 (1988).
[10] F. H. Stillinger and A. Rahman, J. Chem. Phys. **57,** 1281 (1972).
[11] F. H. Stillinger and A. Rahman, J. Chem. Phys. **60,** 1545 (1974).
[12] W. L. Jorgensen and J. D. Madura, Mol. Phys. **56,** 1381 (1985).
[13] J. J. De Pablo and J. M. Prausnitz, Fluid Phase Equilibria **53,** 177 (1989).
[14] S. F. O'Shea and P. R. Tremaine, J. Phys. Chem. **84,** 3304 (1980).
[15] Y. Kataoka, J. Chem. Phys. **87,** 589 (1987).
[16] R. D. Mountain, J. Chem. Phys. **90,** 1866 (1989).
[17] W. L. Jorgensen, J. Chandrasekhar, J. D. Madura, R. W. Impey, and M. L. Klein, J. Chem. Phys. **79,** 926 (1983).
[18] M. P. Allen and D. J. Tildesley, Computer Simulation of Liquids, Oxford University Press, New York 1987.
[19] T. A. Andrea, W. S. Swope, and H. C. Andersen, J. Chem. Phys. **79,** 4576 (1983).
[20] A. G. Kalinichev, in preparation.
[21] A. G. Kalinichev, Int. J. Thermophys. **7,** 887 (1986).
[22] W. L. Jorgensen, J. Chem. Phys. **77,** 4156 (1982).
[23] L. Haar, J. S. Gallagher, and G. S. Kell, NBS-NRC Steam Tables, Hemisphere, Washington, D.C. 1984.
[24] J. Brodholt and B. Wood, Geochimica et Cosmochimica Acta **54,** 2611 (1990).
[25] J. C. Berendsen, J. P. M. Postma, W. F. Van Gunsteren, and J. Hermans, in: Intermolecular Forces (B. Pullman, ed.), Riedel, Dordrecht 1981, p. 331.
[26] J. J. De Pablo, J. M. Prausnitz, H. J. Strauch, and P. T. Cummings, J. Chem. Phys. **93,** 7355 (1990).
[27] V. Carravetta and E. Clementi, J. Chem. Phys. **81,** 2646 (1984).
[28] O. A. Karim and A. D. Haymet, J. Chem. Phys. **89,** 6895 (1988).
[29] D. Hankins, J. W. Moskowitz, and F. H. Stillinger, J. Chem. Phys. **53,** 4544 (1970).
[30] A. Z. Panagiotopoulos, Mol. Phys. **61,** 813 (1987).
[31] M. Rovere, D. W. Heermann, and K. Binder, J. Phys.: Condens. Matter **2,** 7009 (1990).
[32] A. Saul and W. Wagner, J. Phys. Chem. Ref. Data **18,** 1537 (1989).
[33] W. L. Jorgensen, Chem. Phys. Lett. **92,** 405 (1982).
[34] B. Jayaram and D. L. Beveridge, J. Phys. Chem. **94,** 7288 (1990).
[35] P. Bopp, G. Jancso, and K. Heinzinger, Chem. Phys. Lett. **98,** 129 (1983).
[36] H. Tanaka and I. Ohmine, J. Chem. Phys. **87,** 6128 (1987).
[37] Yu. E. Gorbaty and Yu. N. Demianets, Chem. Phys. Lett. **100,** 450 (1983); Mol. Phys. **55,** 571 (1985).
[38] A. K. Soper and M. G. Phillips, Chem. Phys. **107,** 47 (1986).
[39] E. Clementi, J. Phys. Chem. **89,** 4426 (1985).
[40] M. F. Holovko, Yu. V. Kalyuzhny, and K. Heinzinger, Z. Naturforsch. **45a,** 687 (1990).